Available online at www.sciencedirect.com
ScienceDirect
Journal of Power Sources 176 (2008) 417–425
JOURNAL OF POWER SOURCES
www.elsevier.com/locate/jpowsour

Understanding $RuO_2 \cdot xH_2O$/carbon nanofibre composites as supercapacitor electrodes

F. Pico [a], J. Ibañez [b], M.A. Lillo-Rodenas [c], A. Linares-Solano [c], R.M. Rojas [a], J.M. Amarilla [a], J.M. Rojo [a,*]

[a] *Instituto de Ciencia de Materiales de Madrid (ICMM), Consejo Superior de Investigaciones Cientificas (CSIC), Cantoblanco, Sor Juana Ines de la Cruz 3, E-28049 Madrid, Spain*
[b] *Centro Nacional de Investigaciones Metalurgicas, CSIC, Avda Gregorio del Amo 8, E-28040 Madrid, Spain*
[c] *MCMA, Departamento de Quimica Inorganica, Universidad de Alicante, P.O. Box 99, E-03080 Alicante, Spain*

Received 14 August 2007; received in revised form 31 October 2007; accepted 1 November 2007

Abstract

Composites made from $RuO_2 \cdot xH_2O$ particles supported on carbon nanofibres (CNF) have been prepared for supercapacitor electrodes. CNF, produced by Grupo Antolin Ing. SA. using a floating catalyst procedure was treated either in HCl or in HNO_3. Then the composites were obtained by impregnation of CNF with an aqueous $RuCl_3 \cdot 0.5H_2O$ solution followed by filtering and alkali solution treatment. Heat treatment at 150 °C for 2 h was done. Specific capacitance of the composites has been measured and discussed on the basis of their $RuO_2 \cdot xH_2O$ content and $RuO_2 \cdot xH_2O$ particle size. The composites having $RuO_2 \cdot xH_2O$ contents below 11 wt% show $RuO_2 \cdot xH_2O$ particles, which grow from 2 to 4 nm as the $RuO_2 \cdot xH_2O$ content increases. The specific capacitance of supported $RuO_2 \cdot xH_2O$, which can be very high (up to 840 F g^{-1}), decreases as the $RuO_2 \cdot xH_2O$ content increases and $RuO_2 \cdot xH_2O$ particles grow. The composites having $RuO_2 \cdot xH_2O$ contents above 11 wt% show $RuO_2 \cdot xH_2O$ particles of nearly constant size (4 nm); the effect of increasing the $RuO_2 \cdot xH_2O$ content is to increase the amount of particles but not the size of the particles. In these composites the specific capacitance of supported $RuO_2 \cdot xH_2O$ is nearly constant (440 F g^{-1}) and close to bare $RuO_2 \cdot xH_2O$ (460 F g^{-1}).

Keywords: Carbon nanofibres; Hydrous ruthenium oxide; Composites; Supercapacitors

1. Introduction

Since the pioneer work by Miller et al. [1] in which ruthenium oxide nanoparticles were deposited on carbon aerogels, numerous works have dealt with this matter [2–26]. In all of them the objective was to combine the pseudocapacitance (also called redox-type capacitance) of ruthenium oxide with the double-layer capacitance of a carbon in order to take in advantage from the contribution of the two materials and to get high-capacitance ruthenium oxide/carbon composites. Indeed, the composites showed specific capacitances higher than those of the carbons itself. Assuming that the specific capacitance of the composites follows the rule of mixtures, specific capacitances for hydrous ruthenium oxide (usually named $RuO_2 \cdot xH_2O$) as high as 1000 F g^{-1}, i.e. even higher than that of bare $RuO_2 \cdot xH_2O$ (720 F g^{-1}) [27], have been reported [7,9,10,15,19,22]. This fact has opened the possibility of achieving very high-capacitance electrode composites.

Despite the great effort done on preparing $RuO_2 \cdot xH_2O$/carbon composites, e.g. by different procedures, with different carbons (activated carbons, mesoporous carbons, carbon aerogel, carbon black, carbon nanotubes, etc.), with different contents in RuO_2, and by applying different annealing temperatures, several questions remain opened. For instance, how the specific capacitance of the composites and how the specific capacitance of supported $RuO_2 \cdot xH_2O$ depend on the $RuO_2 \cdot xH_2O$ content [1,3,4,7,9,10,12,17,22–24], or why the specific capacitance of supported $RuO_2 \cdot xH_2O$ seems to change with the carbon chosen as support for a given RuO_2 content [10,16]. These questions point out that an understanding of the specific capacitance of the composites and the specific capacitance of the supported $RuO_2 \cdot xH_2O$ is still lacking.

* Corresponding author.
E-mail address: jmrojo@icmm.csic.es (J.M. Rojo).

0378-7753/$ – see front matter © 2007 Elsevier B.V. All rights reserved.
doi:10.1016/j.jpowsour.2007.11.001

Regarding carbon nanofibres [28–32], which are the support chosen in this work, only a few ruthenium oxide/carbon nanofibres composites have been prepared by electrospinning. Hence articles dealing with this type of composites are rather scarce [26]. In general carbon nanofibres (CNF) show: (i) moderate specific double-layer capacitance (1–50 F g^{-1} in aqueous electrolyte) because of their small specific surface area (10–200 m^2 g^{-1}) [28,29] and (ii) high electric conductivity (1×10^3 S cm^{-1}) because of their highly ordered structure [33]. The small surface area would be a drawback limiting the maximum amount of supported ruthenium oxide. The high conductivity, however, is an advantage to get electrodes with high electric conductivity. Compared to other carbons such as activated carbons or mesopore-templated carbons, CNF have been chosen as support because: (i) the specific capacitance of CNF and that of $RuO_2{\cdot}xH_2O$ are very different; it has allowed us to do an accurate study on the variation of the composite specific capacitance as a function of the $RuO_2{\cdot}xH_2O$ content, (ii) $RuO_2{\cdot}xH_2O$/CNF composites are simple composites; because they are easily compacted and show high electric conductivity, neither an inert binder nor an electric conductor are needed to be added to the composites, and (iii) the choice of CNF as support has made easy the study by TEM on the distribution of supported $RuO_2{\cdot}xH_2O$ particles; CNF and $RuO_2{\cdot}xH_2O$ show different shapes and contrasts. Compared to carbon nanotubes (either SWCNT or MWCNT), CNF are cheaper.

In this work $RuO_2{\cdot}xH_2O$ (where x seems to depend on the heating treatment done [27]) has been deposited on CNF following an impregnation method. The composites have been structurally and texturally characterized. Their specific capacitance has been discussed in relation to the $RuO_2{\cdot}xH_2O$ content and $RuO_2{\cdot}xH_2O$ particle size.

2. Experimental

Carbon nanofibres (CNF) were produced by a catalytically vapour-grown procedure in Grupo Antolin Ing. SA., and supplied by the same company. They are highly graphitic cup-stacked fibres showing non-amorphous carbon coating, large hollow core and ca. 100 nm diameter [34]. These CNF, labelled as GANF1 in reference [34], were acid-treated (HCl or HNO_3) and were used in this work as support for the $RuO_2{\cdot}xH_2O$ particles.

Three grams of CNF was dispersed either in 200 ml of 12 M HCl or in 200 ml of 13 M HNO_3, and the dispersions were heated under refluxing at 98 °C for 4 h. The dispersions were filtered and the solids were exhaustively washed with distilled water. The solids were dried at 80 °C overnight. The samples of CNF-treated in HCl or in HNO_3 are hereafter referred as CNF-HCl or CNF-HNO_3, respectively.

0.5 g of either CNF-HCl or CNF-HNO_3 was dispersed in 50 ml of an aqueous 0.034 M $RuCl_3{\cdot}0.5H_2O$ solution under continuous stirring for 24 h. In some particular cases, and in order to get impregnations with very low contents in $RuCl_3{\cdot}0.5H_2O$, lower concentrations (i.e. 0.017 and 0.0015 M) of the $RuCl_3{\cdot}0.5H_2O$ solution were used such as other authors did [8]. In all cases the dispersions were filtered to remove the $RuCl_3{\cdot}0.5H_2O$ solution excess and to get carbon nanofibres impregnated with those solutions. Then the impregnated carbon nanofibres were added to 50 ml of aqueous 10^{-4} M NaOH solution and the pH was measured. Drop wise of another 0.01 M NaOH solution was added to neutralize the dispersion (up to pH 7), then formation of $RuO_2{\cdot}xH_2O$ happened. The dispersions were filtered and the solids were collected. They were washed with distilled water up to negative chloride test. Finally, the composites either $RuO_2{\cdot}xH_2O$/CNF-HCl or $RuO_2{\cdot}xH_2O$/CNF-HNO_3 were dried at 80 °C overnight.

Accumulative treatments consisting of impregnations of both CNF-HCl or CNF-HNO_3 with the 0.034 M $RuCl_3{\cdot}0.5H_2O$ solution followed by filtering and neutralization in 0.01 M NaOH solution were done in order to increase the loading in $RuO_2{\cdot}xH_2O$. The composites are hereafter referred as $n$$RuO_2{\cdot}xH_2O$/CNF-HCl or $n$$RuO_2{\cdot}xH_2O$/CNF-$HNO_3$, where n stands for the number of accumulative treatments done. Using $RuCl_3{\cdot}0.5H_2O$ solutions of lower concentrations (0.017 or 0.0015 M) we got composites having $RuO_2{\cdot}xH_2O$ loadings lower compared to the composites at $n = 1$.

A sample of bare $RuO_2{\cdot}xH_2O$ was also prepared by adding drop wise of 0.01 M NaOH solution on 50 ml of 0.034 M $RuCl_3{\cdot}H_2O$ solution; the added volume of the 0.01 M NaOH solution was that needed to increase the pH solution up to pH 7. The solid obtained, i.e. $RuO_2{\cdot}xH_2O$, was washed with distilled water and then air-dried at room temperature.

All the samples studied in this work, i.e. CNF-HCl, CNF-HNO_3, composites, and bare $RuO_2{\cdot}xH_2O$, were heat-treated at 150 °C for 2 h.

Infrared (IR) spectra were recorded in Bruker IFS 66v/S equipment. KBr-based pellets were prepared by mixing either CNF-HCl or CNF-HNO_3 with dried KBr and then by compacting under a pressure of 2 tonnes cm^{-2}. The relative weight content of CNF-HCl or CNF-HNO_3 in the pellets was nearly 2 wt%.

Temperature-programmed desorption (TPD) experiments were carried out on the CNF-HCl and CNF-HNO_3 samples in a DSC-TG equipment (TA Instruments, SDT 2960 Simultaneous) coupled to a mass spectrometer (Thermostar, Balzers, GSD 300 T3), to characterize the surface chemistry of the samples. In these experiments 10 mg were heated up to 900 °C (heating rate 20 °C min^{-1}) under helium flow rate of 100 ml min^{-1}.

Thermogravimetric (TG) analyses were carried out in air-flow (50 ml min^{-1}) at a heating rate of 5 °C min^{-1} with a Seiko Exstar 6300 instrument. In all cases the mass of the composite was of ca. 20 mg.

X-ray powder diffraction (XRD) patterns were recorded at room temperature in a D-8 Bruker diffractometer, with Cu Kα radiation. The XRD patterns were obtained in the step scanning mode of 0.02° (2θ) and 1 s/step counting time, within the range $10 \leq 2\theta \leq 70°$. The average crystallite size was calculated from the full width at half maximum (FWHM) of several diffraction lines by applying the Scherrer equation:

$$D = \frac{\lambda}{\beta \cos\theta} \quad (1)$$

where λ is the wavelength of the X-rays, θ is the diffraction angle, and $\beta = \sqrt{(\beta_m^2 - \beta_s^2)}$ is the corrected FWHM, where β_m is the FWHM of the experimental diffraction lines, and β_s is the FWHM of the diffraction lines of a standard sample.

Nitrogen adsorption/desorption isotherms were measured at 77 K using an automatic adsorption system (Autosorb-6B, Quantachrome). The samples were outgassed at 110 °C for 4 h. From the adsorption isotherms BET was applied.

Transmission electron micrographs (TEMs) were taken in Jeol JEM 2010 FX and Jeol 3000 EX microscopes operating at acceleration voltages of 200 and 300 kV, respectively. The samples were dispersed in *n*-butyl alcohol, and drops of the dispersions were transferred to a carbon-coated copper grid.

Supercapacitor electrodes were processed as cylindrical pellets of 13 mm diameter and ca. 1 mm height. Compaction of the active $RuO_2{\cdot}xH_2O$/CNF-HCl or $RuO_2{\cdot}xH_2O$/CNF-HNO_3 composites was done at a pressure of 38 MPa. It was not necessary to add either a binder (a polymer) to improve pellets compaction or a good electric conductor (carbon black) to improve electric conductivity. Electric conductivity of parallelepiped electrodes, also compacted at 38 MPa, was measured by a conventional four-probe method in which a current was applied at the two outer probes and voltage drop was measured at the two inner probes; a silver paint was used to get the four probes on the parallelepiped pellets. Supercapacitors were assembled in two-electrode Swagelok™-type cells. The two cylindrical electrodes were separated by a glassy microfibre paper (Whatman 934 AH). Aqueous 2 M H_2SO_4 solution was chosen as electrolyte. Two tantalum rods acted as current collectors. Charge and discharge of the supercapacitor cells were followed by galvanostatic measurements at room temperature on a 1286 Solartron potentiostat/galvanostat.

3. Results and discussion

3.1. Structural and thermal characterization

The acid treatment done (either HCl or HNO_3) on the CNF removes nickel particles accompanying CNF, as deduced from XRD (patterns not shown). The nickel particles come from the catalyst used along the synthesis of CNF. We applied these acid treatments because we know that while HCl does not oxidize carbons, HNO_3 does it.

IR spectra of the CNF-HCl and CNF-HNO_3 samples, in the frequency region of 1500–2000 cm^{-1}, are shown in Fig. 1. The spectrum of the CNF-HNO_3 sample shows bands at 1580 and 1630 cm^{-1} that are ascribed to stretching C=C and C=O vibrations, respectively; the former band comes from the graphene structure of the nanofibres, the latter one comes from acetone-like groups that are placed at the nanofibres surface. The band at 1630 cm^{-1} could have some contribution from adsorbed water. In addition to the two mentioned bands, the spectrum shows another band at 1720 cm^{-1} that can be ascribed to stretching C=O vibrations from carboxyl groups (COOH) at the nanofibre surface. The three bands are also observed in the IR spectrum of CNF-HCl. However the higher intensity of the 1720 cm^{-1} band at the CNF-HNO_3 spectrum confirms that the HNO_3 treatment has given way to new carboxyl groups, in agreement with other reports [16].

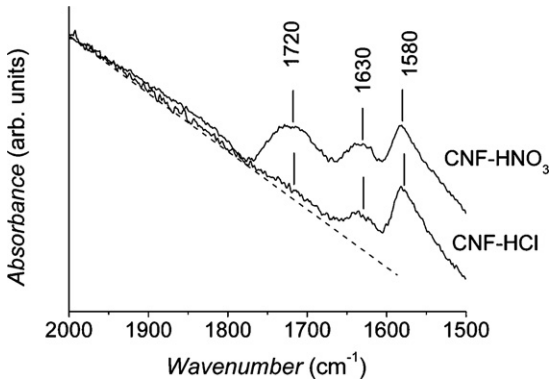

Fig. 1. IR spectra, in the 2000–1500 cm^{-1} region, of the carbon nanofibres heat-treated in HCl (CNF-HCl) or in HNO_3 (CNF-HNO_3). Dashed line stands for the spectra base line.

To estimate the content in basic CO groups and acidic COOH ones in the two carbon nanofibres (CNF-HCl and CNF-HNO_3), TPD measurements were carried out on these samples (Fig. 2). In this figure we see the curves due to evolution of gases CO and CO_2 coming from the carbon nanofibres upon heat treatment [35,36]. From the integrated intensities of the observed peaks, the amounts of CO and CO_2, and hence the amounts of basic CO and acidic COOH groups have been determined. The content in basic groups is close for the two samples (0.33 mmol g^{-1}

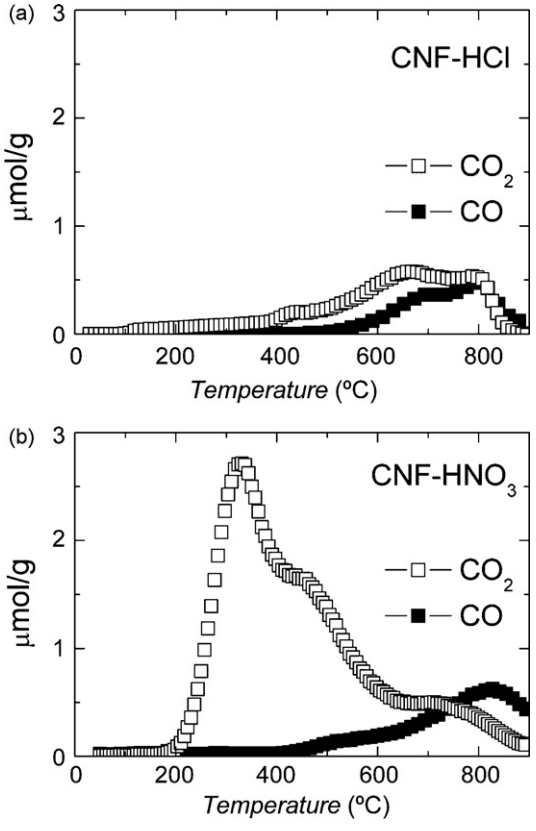

Fig. 2. TPD curves corresponding to CO and CO_2 evolution in CNF-HCl (a) and CNF-HNO_3 (b).

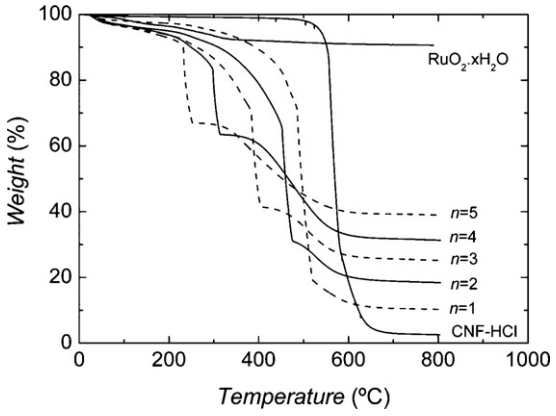

Fig. 3. TG analyses (in air-flow) obtained on several nRuO$_2$·xH$_2$O/CNF-HCl composites heat-treated at 150 °C for 2 h. The TG curves of starting CNF-HCl and bare RuO$_2$·xH$_2$O, both previously heat-treated at 150 °C for 2 h, are included as references.

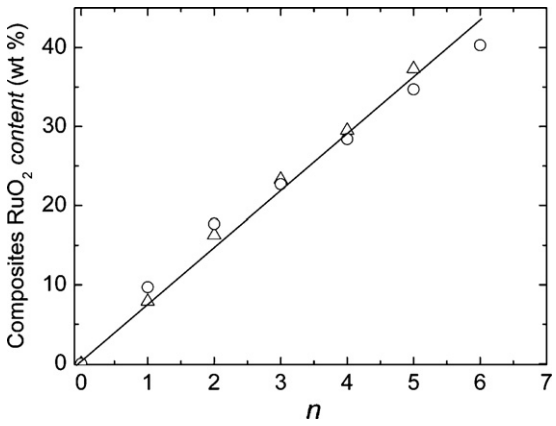

Fig. 4. Variation of the composite RuO$_2$ content (in wt%) vs. the number (n) of accumulative treatments (impregnation + filtering + neutralization) done. Triangles and circles stand for nRuO$_2$·xH$_2$O/CNF-HCl composites and nRuO$_2$·xH$_2$O/CNF-HNO$_3$ ones, respectively. Straight line is the best linear fit found.

for CNF-HCl and 0.44 mmol g^{-1} for CNF-HNO$_3$). However, the content in acidic groups is clearly higher for the CNF-HNO$_3$ sample (0.60 mmol g^{-1} for CNF-HCl and 2.1 mmol g^{-1} for CNF-HNO$_3$). The HNO$_3$ treatment, as expected, has oxidized CNF and increased the content in COOH groups.

In Fig. 3 we show the air-flow TG curves recorded for CNF-HCl, some nRuO$_2$·xH$_2$O/CNF-HCl composites, and bare RuO$_2$·xH$_2$O. For CNF-HCl we see a weight loss at about 600 °C that is due to combustion of the carbon nanofibres. The low weight% residue (plateau observed between 700 and 800 °C) accounts for a low ash content after combustion. For nRuO$_2$·xH$_2$O/CNF-HCl composites we see a sharp weight loss due to combustion of carbon nanofibres; the combustion temperature decreases as n increases pointing out that combustion of the carbon nanofibres is favoured by the amount of supported RuO$_2$·xH$_2$O. It agrees with the fact that RuO$_2$·xH$_2$O catalyses combustion of carbons [12,37]. The residues at the high-temperature plateaux are ascribed to ash from the carbon nanofibres plus crystalline RuO$_2$ (rutile-type structure); the latter is evidenced by XRD (pattern not shown). Taking into account the weight of the residue of the starting CNF-HCl and the weight of the residues of the nRuO$_2$·xH$_2$O/CNF-HCl composites, the RuO$_2$ content in each composite has been determined (Table 1). In Fig. 3 the TG curve of bare RuO$_2$·xH$_2$O shows: (i) a weight loss up to 150 °C that is ascribed to removal of adsorbed water without crystallization of the oxide, (ii) a plateau between 150 and 250 °C, and (iii) another small weight loss above 250 °C due to removal of additional water; it is accompanied by crystallization of the amorphous RuO$_2$·xH$_2$O giving rise to crystalline RuO$_2$ with rutile-type structure [27]. Hence, the high-temperature plateau is ascribed to crystalline RuO$_2$. From the relative contents in water and in RuO$_2$, we have estimated $x = 0.76$ in our RuO$_2$·xH$_2$O sample. We have also estimated the RuO$_2$·xH$_2$O ($x = 0.76$) content in our composites from the TG results (Table 1).

Variation of the RuO$_2$ content vs. n is shown in Fig. 4 for the composites nRuO$_2$·xH$_2$O/CNF-HCl (triangles) and nRuO$_2$·xH$_2$O/CNF-HNO$_3$ (circles). Despite the different content in COOH groups of CNF-HCl and CNF-HNO$_3$, we surprisingly observe that, in the two cases, the RuO$_2$ content increases linearly with the number of treatments (impregnation + filtering + neutralization) done. From the slope we deduce that nearly 7 wt% RuO$_2$ is loaded per treatment. In Fig. 4 we also see that it is possible to achieve RuO$_2$ contents as high as 40% by weight after six accumulative treatments.

Because bare RuO$_2$·xH$_2$O remains amorphous after heating at 150 °C and at this temperature shows its highest

Table 1
RuO$_2$ and RuO$_2$·xH$_2$O contents (in wt%), and electric conductivity (in S cm^{-1}) of the nRuO$_2$·xH$_2$O/CNF-HCl and nRuO$_2$·xH$_2$O/CNF-HNO$_3$ composites

nRuO$_2$·xH$_2$O/CNF-HCl	RuO$_2$ (wt%)	RuO$_2$·xH$_2$O (wt%)	σ (S cm^{-1})	nRuO$_2$·xH$_2$O/CNF-HNO$_3$	RuO$_2$ (wt%)	RuO$_2$·xH$_2$O (wt%)	σ (S cm^{-1})
$n = 0$ (CNF-HCl)	0	0	2.0	$n = 0$ (CNF-HNO$_3$)	0	0	2.7
A	0.8	0.9	–	*A*	2.2	2.4	–
B	4.4	4.8	–	*B*	8.4	9.2	–
$n = 1$	7.9	8.6	4.1	$n = 1$	9.7	10.6	–
$n = 2$	16.3	17.8	–	$n = 2$	17.7	19.3	1.6
$n = 3$	23.3	25.5	–	$n = 3$	22.7	24.8	–
$n = 4$	29.5	32.2	8.6	$n = 4$	28.4	31	–
$n = 5$	37.3	40.8	–	$n = 5$	34.7	37.9	9.2
$n = 6$	–		–	$n = 6$	40.3	44	–
RuO$_2$·xH$_2$O	90.7	100	89	–	–	–	–

n stands for the number of accumulative treatments done, all samples were heat-treated at 150 °C for 2 h, *A* and *B* stand for the composites obtained from low-concentrated RuCl$_3$·0.5H$_2$O solutions.

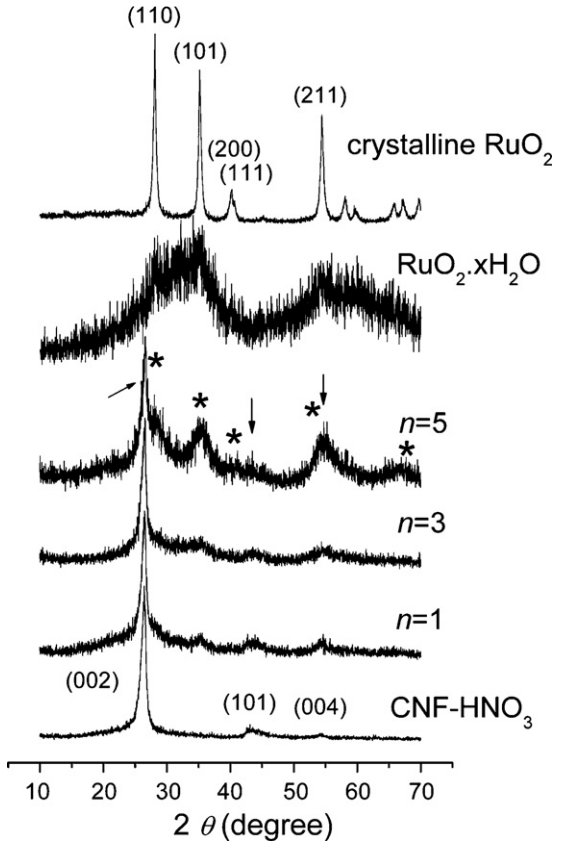

Fig. 5. XRD patterns recorded at rt on several nRuO$_2$·xH$_2$O/CNF-HNO$_3$ composites heat-treated at 150 °C for 2 h. The XRD patterns of CNF-HNO$_3$ and bare RuO$_2$·xH$_2$O after the same heat treatment are included as references. The XRD pattern of crystalline RuO$_2$ is shown as another reference.

specific capacitance [27], our RuO$_2$·xH$_2$O/CNF-HCl and RuO$_2$·xH$_2$O/CNF-HNO$_3$ composites have been heated at 150 °C for 2 h as a standard treatment. XRD patterns of some heat-treated nRuO$_2$·xH$_2$O/CNF-HNO$_3$ composites are shown as examples in Fig. 5. In this figure the XRD patterns of CNF-HNO$_3$, bare RuO$_2$·xH$_2$O and crystalline RuO$_2$ have been included as references. In all composite patterns we see some diffractions lines (arrow marked) that are ascribed to the carbon nanofibres. In addition we see broad and low-intensity diffraction lines (asterisk marked) whose positions coincide with those of crystalline RuO$_2$; these lines indicate some crystallization of supported RuO$_2$·xH$_2$O. From the full width at half maximum (FWHM) of these diffraction lines and by applying the Scherrer equation (Eq. (1)), we have deduced a crystallite size of 4 nm for supported RuO$_2$·xH$_2$O.

3.2. Textural characterization of the composites

Transmission electron micrographs obtained on composites having CNF-HNO$_3$ as support and different loadings in RuO$_2$·xH$_2$O are shown as examples in Fig. 6. Images show RuO$_2$·xH$_2$O particles deposited on the surface of the carbon nanofibres. The particle size is of 2 nm for the composite of low RuO$_2$·xH$_2$O content (Fig. 6a). However the particle size is larger (4 nm) for the composites of higher RuO$_2$·xH$_2$O

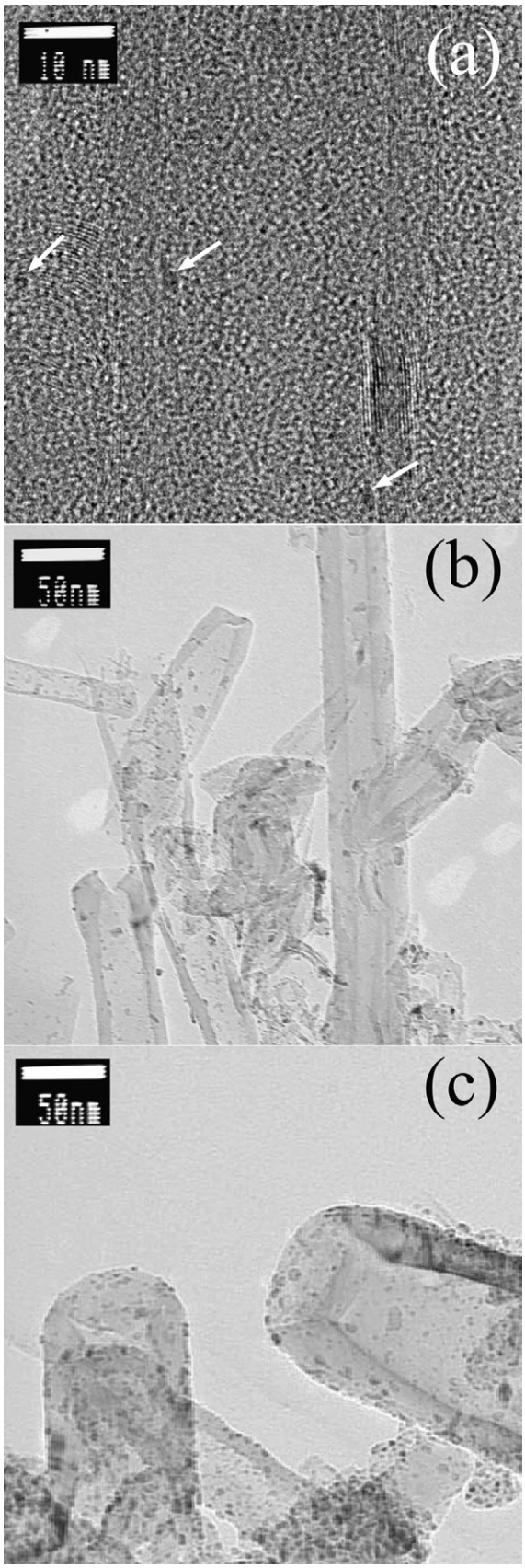

Fig. 6. TEM images obtained on RuO$_2$·xH$_2$O/CNF-HNO$_3$ composites having RuO$_2$·xH$_2$O (x = 0.76) contents of 2.4 wt% (a), 10.6 wt% (b), and 24.8 wt% (c). RuO$_2$·xH$_2$O particles in (a) are arrow marked. Scale is 10 nm in (a), 50 nm in (b), and 50 nm in (c).

contents (Fig. 6b and c); this particle size agrees with the crystallite size deduced from XRD. From comparison of Fig. 6b and c we see that the particle size remains constant (4 nm) but the effect on increasing the $RuO_2{\cdot}xH_2O$ content is to increase the amount of supported $RuO_2{\cdot}xH_2O$ particles. This result agrees with the linear dependence found in Fig. 4 for RuO_2 content vs. number of treatments done. Therefore, particle size of supported $RuO_2{\cdot}xH_2O$ increases from 2 to 4 nm as $RuO_2{\cdot}xH_2O$ loading increases in the range 0–11 wt%, but particle size is nearly constant (4 nm) for $RuO_2{\cdot}xH_2O$ loadings above 11 wt%.

Nitrogen adsorption/desorption isotherms of CNF-HNO_3, $5RuO_2{\cdot}xH_2O$/CNF-HNO_3 and bare $RuO_2{\cdot}xH_2O$ are shown as examples in Fig. 7a. For CNF-HNO_3 and $5RuO_2{\cdot}xH_2O$/CNF-HNO_3 the isotherms are type II, showing at low relative pressures ($P/P_0 < 0.1$) the presence of micropores. At intermediate relative pressures ($P/P_0 = 0.4$–0.7) we see the important mesoporosity contribution. At high relative pressures ($P/P_0 > 0.7$) the hysteresis loops confirm the presence of mesopores, presumably coming from the opened and entangled nanofibres, as well as some macropores. The shape of the $RuO_2{\cdot}xH_2O$ isotherm is quite different showing much lower adsorption capacity.

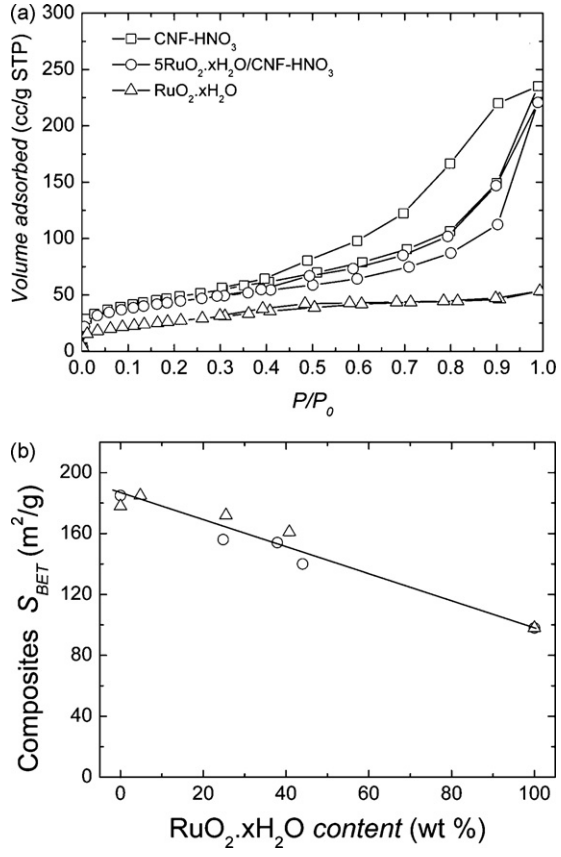

Fig. 7. (a) Nitrogen adsorption/desorption isotherms recorded on the $5RuO_2{\cdot}xH_2O$/CNF-HNO_3 composite, the starting CNF-HNO_3 and the bare $RuO_2{\cdot}xH_2O$. (b) Dependence of the BET specific surface area as a function of the $RuO_2{\cdot}xH_2O$ ($x = 0.76$) content in $RuO_2{\cdot}xH_2O$/CNF-HCl composites (triangles) and $RuO_2{\cdot}xH_2O$/CNF-HNO_3 composites (circles). Straight line is the best fit to Eq. (2).

Variation of the BET specific surface area as a function of the $RuO_2{\cdot}xH_2O$ ($x = 0.76$) content is shown in Fig. 7b for the two kinds of composites. We find a linear dependence according to equation:

$$S_{BET} = (100 - \alpha)\frac{(S_{BET})_1}{100} + \frac{\alpha(S_{BET})_2}{100} \quad (2)$$

where α stands for the weight percentage of $RuO_2{\cdot}xH_2O$, $(100-\alpha)$ stands for the weight percentage of CNF-HCl or CNF-HNO_3, $(S_{BET})_1$ stands for the specific surface area of CNF-HCl or CNF-HNO_3, and $(S_{BET})_2$ stands for the specific surface area of bare $RuO_2{\cdot}xH_2O$. The straight line found indicates that the rule of mixtures holds and the two kinds of composites behave like a mixture of two components (carbon nanofibres and hydrous ruthenium oxide) from the point of view of their specific surface area.

3.3. Electrical and electrochemical characterization.

Electric conductivity of parallelepiped shape electrodes measured at room temperature by the four-probe method is outlined in Table 1. It compiles the conductivity obtained for the starting carbon nanofibres (CNF-HCl and CNF-HNO_3) as well as for some composites ($n RuO_2{\cdot}xH_2O$/CNF-HCl and $n RuO_2{\cdot}xH_2O$/CNF-HNO_3) and for bare $RuO_2{\cdot}xH_2O$. Composites conductivity is in the same order of magnitude (1–10 S cm^{-1}) as carbon nanofibres conductivity (2 and 2.7 S cm^{-1} for CNF-HCl and CNF-HNO_3, respectively). It agrees with the fact that the $RuO_2{\cdot}xH_2O$ content is below percolation threshold [38,39]. For $RuO_2{\cdot}xH_2O$ contents above percolation threshold, the composites conductivity should be close to bare $RuO_2{\cdot}xH_2O$ conductivity (89 S cm^{-1}).

Charge/discharge galvanostatic plot (voltage vs. time) obtained at 23 mA cm^{-2} is shown as an example in Fig. 8a. At the beginning of the charge and the discharge we see a sharp change in voltage (ΔV_1) from which the equivalent series resistance (ESR) of the supercapacitor cell has been determined according to $\Delta V_1 = 2 \times I \times \mathrm{ESR}$. Capacitance of the cell has been measured along the discharge process according to $C = I \times t_d/\Delta V_2$, where t_d and ΔV_2 stand for the discharge time and voltage decrement, respectively. The capacitance (C_e) of each electrode is $C_e = 2C$ in accordance with the series arrangement of the two electrodes within the cell. From C_e and the mass of the electrode (i.e. the mass of the carbon nanofibres, the composites or the bare $RuO_2{\cdot}xH_2O$), the specific capacitance (in F g^{-1}) has been calculated. Variation of the specific capacitance vs. the current density is shown in Fig. 8b. We see that in all cases (i.e. CNF-HCl, $n RuO_2{\cdot}xH_2O$/CNF-HCl composites, and bare $RuO_2{\cdot}xH_2O$) the specific capacitance decreases slightly as the current density increases. This behaviour agrees with the fact that electric conductivity is high enough in all cases [38]. On the other hand, we have checked the cycle life of the composites that is rather high. As an example the supercapacitor cell having the composite $5RuO_2{\cdot}xH_2O$/CNF-HCl as electrode was cycled at a current density of 113 mA cm^{-2}. After 10,000 charge/discharge cycles the capacitance had only decreased by 7%.

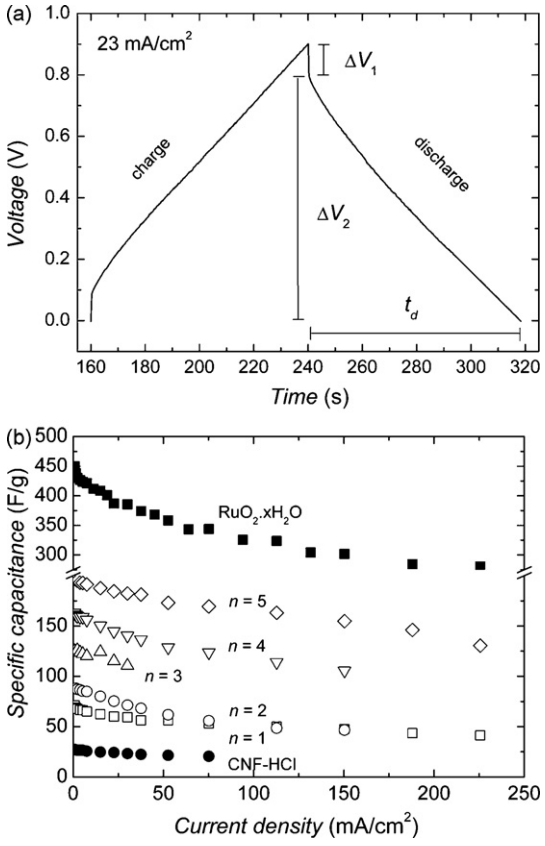

Fig. 8. (a) Galvanostatic charge/discharge plot recorded at 23 mA cm^{-2} for the nRuO$_2$·xH$_2$O/CNF-HCl (n = 4) composite. (b) Dependence of the specific capacitance as a function of the current density for several nRuO$_2$·xH$_2$O/CNF-HCl composites (n = 1, 2, 3, 4 and 5). The dependences found for CNF-HCl and bare RuO$_2$·xH$_2$O are included as references.

The specific capacitance measured at a low current density (1 mA cm^{-2}), i.e. in nearly steady-state, as a function of the RuO$_2$·xH$_2$O (x = 0.76) content has been plotted in Fig. 9 for the two kinds of composites (RuO$_2$·xH$_2$O/CNF-HCl and RuO$_2$·xH$_2$O/CNF-HNO$_3$). Specific capacitance of CNF-HNO$_3$ (32 F g^{-1}) is slightly higher than that of CNF-HCl (27 F g^{-1}) in

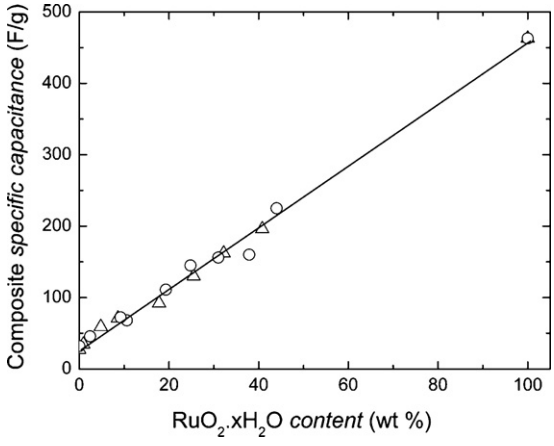

Fig. 9. Composite specific capacitance as a function of the RuO$_2$·xH$_2$O (x = 0.76) content. Triangles and circles stand for RuO$_2$·xH$_2$O/CNF-HCl composites and RuO$_2$·xH$_2$O/CNF-HNO$_3$ ones, respectively. Straight line is the best fit to Eq. (3).

accordance with the higher COOH content of the former sample [40]. In Fig. 9 the specific capacitance of bare RuO$_2$·xH$_2$O has also been included. The experimental data are well-fitted to a straight line in accordance with equation:

$$C_{sp} = (100 - \alpha)\frac{(C_{sp})_1}{100} + \frac{\alpha(C_{sp})_2}{100} \quad (3)$$

where α stands for the RuO$_2$·xH$_2$O (x = 0.76) weight percentage as already mentioned, (100−α) stands for the carbon nanofibres weight percentage, either CNF-HCl or CNF-HNO$_3$, $(C_{sp})_1$ stands for the specific capacitance of CNF-HCl or CNF-HNO$_3$ and $(C_{sp})_2$ stands for the specific capacitance of bare RuO$_2$·xH$_2$O. The fitting by a straight line indicates that the specific capacitance holds the rule of mixtures, i.e. the two kinds of composites behave like a mixture of two components: carbon nanofibres and hydrous ruthenium oxide.

In some RuO$_2$·xH$_2$O/carbon composites a linear dependence of the specific capacitance as a function of the RuO$_2$ content has been reported [1,5,6,10,17]. However in some others, the specific capacitance departs from the linear dependence [3,4,6,7,9,12]. In carbon/carbon composites the specific capacitance follows the rule of mixtures [38], but in composites such as RuO$_2$·xH$_2$O/NiO a loading of 20 wt% RuO$_2$·xH$_2$O is sufficient to get the same specific capacitance as bare RuO$_2$·xH$_2$O [41]. Therefore, the specific capacitance does not follow the same trend in all composites.

In Fig. 9 the intercept of the fitted straight line $(C_{sp})_1$ gives a specific capacitance of 30 F g^{-1} for CNF-HCl and for CNF-HNO$_3$; this value is close to their experimental values (27 and 32 F g^{-1} for CNF-HCl and CNF-HNO$_3$, respectively). From the slope, which is equal to $((C_{sp})_2 - (C_{sp})_1)/100$, we have deduced a specific capacitance of 460 F g^{-1} for bare RuO$_2$·xH$_2$O. From the specific capacitance and the specific surface area (S_{BET}) we have obtained a capacitance per surface area (C_{sp}/S_{BET}) of 15 μF cm^{-2} for CNF-HCl, 17 μF cm^{-2} for CNF-HNO$_3$, and 469 μF cm^{-2} for bare RuO$_2$·xH$_2$O. The two former values agree with values usually reported for a double-layer mechanism (values ranging from 10 to 20 μF cm^{-2})[42–44]. The latter value agrees with a pseudocapacitance mechanism operating in RuO$_2$·xH$_2$O (values reported are usually above 300 μF cm^{-2} depending on the RuO$_2$·xH$_2$O annealing treatment and the electrolyte chosen) [27,41].

Based on the fact that the rule of mixtures holds for the specific capacitance of the two kinds of composites, the specific capacitance of supported RuO$_2$·xH$_2$O has been deduced according to Eq. (3). This magnitude has been plotted as a function of the composite RuO$_2$·xH$_2$O (x = 0.76) content in Fig. 10. For RuO$_2$·xH$_2$O contents below 11 wt% (region I), the specific capacitance of supported RuO$_2$·xH$_2$O is anomalously high (840 F g^{-1}) in agreement with results reported for other RuO$_2$·xH$_2$O/carbon composites [7,9,10,15,19,22]. Moreover, the asymptotic trend observed in region I suggests that it is possible to obtain even higher specific capacitance for supported RuO$_2$·xH$_2$O (i.e. above 840 F g^{-1}) at very low RuO$_2$·xH$_2$O contents. The high specific capacitances found are associated with very small particle size (2 nm) of supported RuO$_2$·xH$_2$O. The decrease of the RuO$_2$·xH$_2$O specific capacitance as the

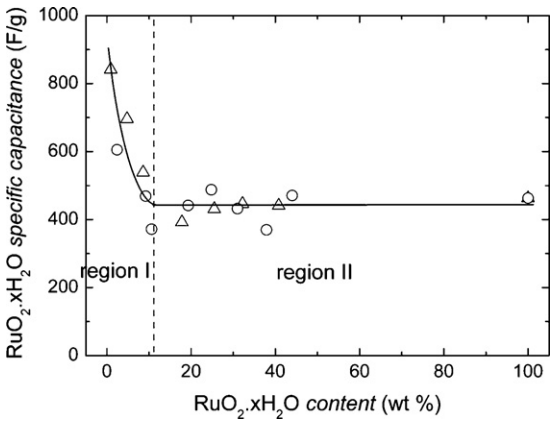

Fig. 10. $RuO_2{\cdot}xH_2O$ specific capacitance vs. $RuO_2{\cdot}xH_2O$ ($x = 0.76$) content in $RuO_2{\cdot}xH_2O$/CNF-HCl composites (triangles) and $RuO_2{\cdot}xH_2O$/CNF-HNO_3 composites (circles). I and II stand for the two regions discussed in the text. Solid line is a guide to the eye.

$RuO_2{\cdot}xH_2O$ content increases indicates that the rule of mixtures fails for composites having low $RuO_2{\cdot}xH_2O$ contents (the depart from the rule of mixtures is not clearly observed in Fig. 9). The decrease in $RuO_2{\cdot}xH_2O$ specific capacitance is associated with an increase in particle size (from 2 to 4 nm) as observed by TEM. For $RuO_2{\cdot}xH_2O$ contents above 11 wt% (region II in Fig. 10) the specific capacitance of supported $RuO_2{\cdot}xH_2O$ is constant, which agrees with the rule of mixtures. In region II, $RuO_2{\cdot}xH_2O$ particle size is constant (4 nm) as observed by TEM. The effect of increasing $RuO_2{\cdot}xH_2O$ content is to increase the amount of supported $RuO_2{\cdot}xH_2O$ particles. The average specific capacitance of supported $RuO_2{\cdot}xH_2O$ (440 F g^{-1}) is close to the specific capacitance of bare $RuO_2{\cdot}xH_2O$ (460 F g^{-1}).

4. Concluding remarks

Composites consisting of $RuO_2{\cdot}xH_2O$ particles deposited on carbon nanofibres have been prepared by accumulative treatments consisting of impregnation of carbon nanofibres with $RuCl_3{\cdot}0.5H_2O$ solution, filtering to remove $RuCl_3{\cdot}0.5H_2O$ excess and neutralization with NaOH solution to get $RuO_2{\cdot}xH_2O$. The procedure has allowed obtaining composites with RuO_2 contents as high as 40 wt%; the amount deposited per treatment is 7 wt% RuO_2.

In composites having $RuO_2{\cdot}xH_2O$ ($x = 0.76$) contents below 11 wt%, the composite specific capacitance departs from the rule of mixtures. $RuO_2{\cdot}xH_2O$ specific capacitance decreases from 840 to 440 F g^{-1} as the particle size increases from 2 to 4 nm. It means that the contribution of $RuO_2{\cdot}xH_2O$ to the specific capacitance of the composite decreases because $RuO_2{\cdot}xH_2O$ particles grow. In composites having $RuO_2{\cdot}xH_2O$ contents above 11 wt% the composite specific capacitance holds the rule of mixtures. $RuO_2{\cdot}xH_2O$ specific capacitance is constant (440 F g^{-1}) in agreement with a constant $RuO_2{\cdot}xH_2O$ particle size (4 nm).

The plot of Fig. 10 seems to be a general plot for carbon-supported $RuO_2{\cdot}xH_2O$ composites. In this plot region I accounts for the dispersion of the supported $RuO_2{\cdot}xH_2O$ particles. Depending on the surface area and porosity of the carbon chosen as support (activated carbon, mesopore-templated carbon, carbon aerogel, carbon nanofibre, etc.), region I would be different in every $RuO_2{\cdot}xH_2O$/carbon composite. This point, however, is unexplored.

Acknowledgements

Financial support trough the project of reference MAT 2005-01606 is gratefully acknowledged. F. Pico thanks for a contract associated with that project. We thank C. Merino, P. Soto and F. Martinez from Grupo Antolin Ing. SA., for providing carbon nanofibres. We thank Mr. Adrian Gomez for technical TEM support.

References

[1] J.M. Miller, B. Dunn, T.D. Tran, R.W. Pekala, J. Electrochem. Soc. 144 (1997) L309.
[2] J.P. Zheng, Electrochem. Solid-State Lett. 2 (1999) 359.
[3] C. Lin, J.A. Ritter, B.N. Popov, J. Electrochem. Soc. 146 (1999) 3155.
[4] R. Ma, B. Wei, C. Xu, J. Liang, D. Wu, Bull. Chem. Soc. Jpn. 73 (2000) 1813.
[5] Y. Sato, K. Yomogida, T. Nanaumi, K. Kobayakawa, Y. Ohsawa, M. Kawai, Electrochem. Solid-State Lett. 3 (2000) 113.
[6] M. Ramani, B.S. Haran, R.E. White, B.N. Popov, L. Arsov, J. Power Sources 93 (2001) 209.
[7] J. Zhang, D. Jiang, B. Chen, J. Zhu, L. Jiang, H. Fang, J. Electrochem. Soc. 148 (2001) A1362.
[8] T. Nanaumi, Y. Ohsawa, K. Kobayakawa, Y. Sato, Electrochemistry 70 (2002) 681.
[9] H. Kim, B.N. Popov, J. Power Sources 104 (2002) 52.
[10] J.H. Park, J.M. Ko, O.O. Park, J. Electrochem. Soc. 150 (2003) A864.
[11] G. Arabale, D. Wagh, M. Kulkarni, I.S. Mulla, S.P. Vernekar, K. Vijayamohanan, A.M. Rao, Chem. Phys. Lett. 376 (2003) 207.
[12] J.H. Jang, S. Han, T. Hyeon, S.M. Oh, J. Power Sources 123 (2003) 79.
[13] V. Panic, T. Vidakovic, S. Gojkovik, A. Dekanski, S. Milonjic, B. Nikolic, Electrochim. Acta 48 (2003) 3805.
[14] X. Qin, S. Durbach, G.T. Wu, Carbon 42 (2004) 451.
[15] W.-C. Chen, C.-C. Hu, C.-C. Wang, C.-K. Min, J. Power Sources 125 (2004) 292.
[16] Y.-T. Kim, K. Tadai, T. Mitani, J. Mater. Chem. 15 (2005) 4914.
[17] M.S. Dandekar, G. Arabale, K. Vijayamohanan, J. Power Sources 141 (2005) 198.
[18] J.-S. Ye, H.F. Cui, X. Liu, T.M. Lim, W.-D. Zhang, F.-S. Sheu, Small 1 (2005) 560.
[19] I.-H. Kim, J.-H. Kim, Y.-H. Lee, K.-B. Kim, J. Electrochem. Soc. 152 (2005) A2170.
[20] C.-C. Wang, C.-C. Hu, Carbon 43 (2005) 1926.
[21] Z. Sun, Z. Liu, B. Han, S. Miao, J. Du, Z. Miao, Carbon 44 (2006) 888.
[22] M. Min, K. Machida, J.H. Jang, K. Naoi, J. Electrochem. Soc. 153 (2006) A334.
[23] G.-Y. Yu, W.-X. Chen, Y.-F. Zheng, J. Zhao, X. Li, Z.-D. Xu, Mater. Lett. 60 (2006) 2453.
[24] J.-K. Lee, H.M. Pathan, K.-D. Jung, O.-S. Joo, J. Power Sources 159 (2006) 1527.
[25] Y. Zhao, L. Liu, J. Xu, J. Yang, M. Yan, Z. Jiang, J. Solid-State Electrochem. 11 (2007) 283.
[26] Y.W. Ju, G.-R. Choi, H.-R. Jung, C. Kim, K.-S. Yang, W.-J. Lee, J. Electrochem. Soc. 154 (2007) A192.
[27] J.P. Zheng, P.J. Cygan, T.R. Jow, J. Electrochem. Soc. 142 (1995) 2699.
[28] S.H. Yoon, S. Lim, Y. Song, Y. Ota, W. Qiao, A. Tanaka, I. Mochida, Carbon 42 (2004) 1723.
[29] C. Merino, P. Soto, E. Vilaplana-Ortego, J.M. Gomez de Salazar, F. Pico, J.M. Rojo, Carbon 43 (2005) 551.

[30] X.Y. Tao, X.B. Zhang, L. Zhang, J.P. Cheng, F. Liu, J.H. Luo, Z.Q. Luo, H.J. Geise, Carbon 44 (2006) 1425.
[31] A.K. Cuentas, M.E. Rincon, J. Power Sources 162 (2006) 743.
[32] N.C. Hung, I.V. Anoshkin, E.G. Rakov, Russ. J. Appl. Chem. 80 (2007) 443.
[33] M. Endo, Y.A. Kim, T. Hayashi, K. Nishimura, T. Matusita, K. Miyashita, M.S. Dresselhaus, Carbon 39 (2001) 1287.
[34] I. Martín-Gullon, J. Vera, J.A. Conesa, J.L. Gonzalez, C. Merino, Carbon 44 (2006) 1572.
[35] M.J. Bleda-Martinez, J.A. Macia-Agullo, D. Lozano-Castello, E. Morallon, D. Cazorla-Amoros, A. Linares-Solano, Carbon 43 (2005) 2677.
[36] Y.-R. Nian, H. Teng, J. Electrochem. Soc. 149 (2002) A1008.
[37] D.W. Mckee, Carbon 8 (1970) 623.
[38] F. Pico, C. Pecharroman, A. Anson, M.T. Martinez, J.M. Rojo, J. Electrochem. Soc. 154 (2007) A579.
[39] S. Mandal, J.M. Amarilla, J. Ibañez, J.M. Rojo, J. Electrochem. Soc. 148 (2001) A24.
[40] E. Raymundo-Piñero, F. Leroux, F. Beguin, Adv. Mater. 18 (2006) 1877.
[41] F. Pico, J. Ibañez, T.A. Centeno, C. Pecharroman, R.M. Rojas, J.M. Amarilla, J.M. Rojo, Electrochim. Acta 51 (2006) 4693.
[42] H. Shi, Electrochim. Acta 41 (1996) 1633.
[43] G. Gryglewicz, J. Machnikowski, E. Lorenc-Grabowska, G. Lota, E. Frackowiak, Electrochim. Acta 50 (2005) 1197.
[44] J. Chmiola, G. Yushin, Y. Gogotsi, C. Portet, P. Simon, P.L. Taberna, Science 313 (2006) 1760.